

Photovoltaic Bypass Diode Fault Detection Using Artificial Neural Networks

Mahmoud Dhimish[✉], Member, IEEE, and Andy M. Tyrrell[✉], Life Senior Member, IEEE

Abstract—Due to the importance of determining faulty bypass diodes in photovoltaic (PV) systems, faulty bypass diodes have been of widespread interest in recent years due to their importance in improving PV system durability, operation, and overall safety. This article presents new work in developing an artificial intelligence (AI) based model using the principles of artificial neural networks (ANNs) to detect short and open PV bypass diode fault conditions. With only three inputs from the PV system, namely, the output power, short-circuit current, and open-circuit voltage, the developed ANN model can determine whether the PV bypass diodes are defective. In the experimentally validated case of short and open bypass diodes, 93.6% and 93.3% of faulty bypass diodes can be detected. Furthermore, the developed ANN model has an average precision and sensitivity of 96.4% and 92.6%, respectively.

Index Terms—Artificial intelligence (AI), bypass diodes, fault detection algorithm, photovoltaics (PVs).

NOMENCLATURE

ANN	Artificial neural network.
ANFIS	Adaptive neuro-fuzzy inference system.
w_{ij}	ANN network neurons.
x_j	ANN network inputs.
w_{j0}	ANN network activation threshold.
b	ANN network bias.
f_1	ANN network non-linear function.
$I-V$	Current–voltage.
I_{MPP}	Current at maximum power point.
FP	False positive rate.
kNN	k -nearest neighbors network.
MPP	Maximum power point.
MLP	Multilayer perceptron.
P_{MPP}	Power at maximum power point.
V_{OC}	Open-circuit voltage.
PV	Photovoltaic.
PID	Potential induced degradation.
$P-V$	Power–voltage.
RBF	Radial basis function.
STC	Standard test conditions.
I_{SC}	Short-circuit current.
TP	True positive rate.
V_{MPP}	Voltage at maximum power point.

Manuscript received 15 November 2022; accepted 19 January 2023. Date of publication 13 February 2023; date of current version 28 February 2023. The Associate Editor coordinating the review process was Dr. Yau Chung. (*Corresponding author: Mahmoud Dhimish.*)

The authors are with the School of Physics, Engineering and Technology, University of York, YO10 5DD York, U.K. (e-mail: mahmoud.dhimish@york.ac.uk; andy.tyrrell@york.ac.uk).

Digital Object Identifier 10.1109/TIM.2023.3244230

I. INTRODUCTION

SOLAR PV energy has shown a worldwide expansion over the past years. So far, the cumulative global installed capacity has exceeded 760 GW [1]. There are increasing global expectations of energy production through solar PV systems. Given its recent expansion, it is crucial to ensure the performance and reliability of such systems. PV power plants operate under the threat of various fault conditions, which will decrease their efficiency, reliability, and lifetime, or even lead to a dangerous operation “fire incident” in some circumstances [2].

The fundamental PV modules are central units of a PV system, and frequently, they are subjected to hardware faults. Such faults can be temporary or permanent, depending on the source [3], and there are various fault types such as mismatch conditions, module aging, PID [4], shading, short-circuit faults [5], and bypass diode faults [6].

The deficiency of bypass diodes can heat the solar cells, causing hotspots, burn marks, and fires in the worst-case scenario [7]. It is hence crucial to identify and correct a bypass diode fault occurrence on a PV module. In contrast, the bypass diode faults can manifest in two situations: open circuit and short circuit. Short-circuit faults can result from bad connections with solar cells or manufacturing defects. On the other hand, open-circuit faults may occur from a disconnection, mainly due to poor soldering and line-to-line faults [8].

Recent studies have identified several fault detection methods and have been explored in the literature. It is possible to categorize these methods into two categories: electrical and non-electrical methods. Electrical methods are usually considered and potentially mitigated using statistical [9], [10] or signal processing methods [11]. For example, Jalil et al. [9] have proposed an enhanced Cassie–Mayr-Based approach for detecting dc series arcing in PV systems. However, the same problem was investigated by [10] by adopting a neural network and receiving signal strength indicators. Both [10] and [11] show accurate results in detecting the dc arcing fault; however, they cannot identify failure in the PV modules’ bypass diodes. A similar precise detection method was developed by [11] to detect line–line and line–ground PV faults using a senseless algorithm based on the acquired data of the PV modules. Again, this method cannot detect faulty PV bypass diodes, which can misidentify the line–ground faults scenario.

The non-electrical methods mainly utilize machine learning-based techniques. Some of these techniques detect the fault

predictively, avoiding potential power losses and damages [5]. However, the most common methods identify and diagnose fault conditions in real-time. For example, Li et al. [12] proposed an ANN to identify and localize PV module degradation, short-circuited and shading about real-time machine learning methods. The input variables are ambient temperature, voltage, and current at the MPP. However, the method was not experimentally tested. In contrast, Bonsignore et al. [13] developed an ANFIS-based algorithm trained using a simulated dataset. This method identifies and diagnoses line-to-line faults, partial shading, and short-circuited bypass diodes. However, experimental tests were not conducted.

The research developed by Madeti and Singh [14] applied a *k*NN to detect short-circuited modules, line-to-line faults, shading, and bypass diode defects. They used ambient temperature, irradiance, and voltage and current at the MPP. This algorithm was not experimentally tested, and their findings showed a maximum error of 3%. Recently, Hussain et al. [15] compared an RBF and an MLP for detecting short-circuited PV modules. Using power and irradiance as input variables, the authors reached a maximum accuracy of 97.9% for the RBF algorithm on the experimental tests. In contrast, there is not any existing PV fault detection algorithm that can detect short-circuit bypass diode fault conditions. There are some attempts from the industry to explain this faulty situation, yet no proposals have practically been utilized.

In point of the case, even when the PV modules suffer from faulty bypass diodes, they typically do not show the impact when no shading/overcasting/clouds affect the modules. The reason behind this, electrically speaking, is that the bypass diodes are only activated during shading conditions. For example, recent studies [16], [17], [18] have shown that partial shading can drop the PV output power; however, it can be effectively alleviated when bypass diodes are equipped with the modules. In addition, the faulty conditions of PV modules, such as faults in bypass diodes or dc arcing, can result in current leakage. For example, Shabani and Mazlumi [19] proposed a communication-assisted overcurrent protection scheme for PV-based dc microgrids, and in a recent review article [20], it was summarized that PV defects such as hotspots or cracks can also lead to leakage of the PV modules and can be somewhat mitigated using integrable power electronics devices.

The problem of PV faults can seriously lead to health and safety concerns about PV technology, ultimately impacting the delivery of the global vision of net-zero carbon by 2050. Therefore, a significant work [21] studied the protection against electric shock in a PV generator (PVG), the dc side of a PV installation. And since then, hundreds of related PV fault detection articles have been proposed in the literature.

This article aims to demonstrate the development of an ANN-based model to detect simultaneously short and open bypass diode fault conditions. With this aim in mind, the article's main contributions are as follows:

- 1) Introduce a simple yet highly accurate ANN-based model that only requires a minimal number of input parameters, namely, PV output power, V_{OC} and I_{SC} , to detect PV bypass diode faults.

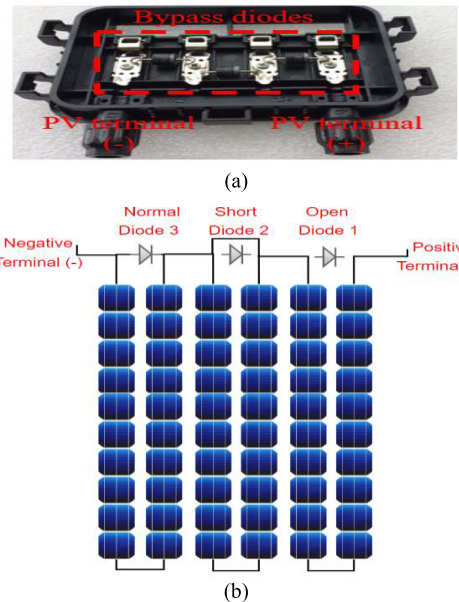


Fig. 1. (a) PV junction box combining three bypass diodes. (b) Snapshot of bypass diodes conditions: open, short, and normal operation.

- 2) Identify the number of faulty PV bypass diodes using the same ANN network without additional input requirements.
- 3) The ANN model comprises a "bias" parameter which allows the use of the model with small-to-medium PV systems capacity.
- 4) Experimentally validate the proposed solution and provide insights for the ANN model precision and sensitivity rates.

This article is organized as follows: Section II introduces the PV bypass diode failure modes, while Section III presents the methodology concepts and theoretical grounds of the developed ANN model. Section IV shows the algorithm's results using different experimental case studies, and finally, Section V concludes the work.

II. PV BYPASS DIODES FAILURE MODES

Traditional and modern PV modules are integrated with bypass diodes, where three to four bypass diodes in the junction box [see Fig. 1(a)] are connected in parallel with the PV sub-strings. The bypass diodes function as an alternative route for the output-generated current when the solar cells in the sub-string(s) are being affected by shading. In other words, they restrict the reverse-biased voltage developed across the partially shaded cells, improving the PV module's overall power production.

Bypass diodes have two main failure modes, failing in open-circuit or in short-circuit, demonstrated in Fig. 1(b). If a bypass diode fails open (Diode1), it can no longer pass a current (complete breakdown). In this case, the diode should be replaced as soon as possible since, in this faulty condition, the sub-string would be affected by heating (known as hotspots) during partial shading conditions. On the contrary, if the bypass diodes fail to short-circuit (Diode2), the solar cells within the sub-string would not contribute to the output voltage

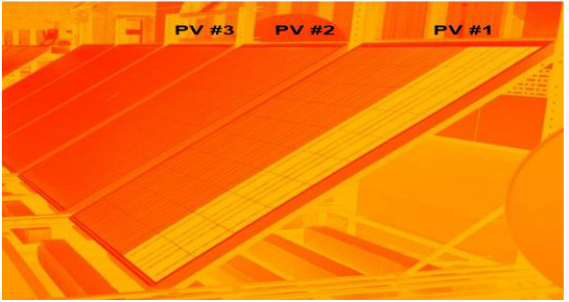


Fig. 2. Thermal image of the three tested PV modules.

for the entire PV module. It would result in a significant drop in the module's output power. It is worth also noting that in this article, the tested modules have three bypass diodes [as in Fig. 1(a)], and each diode is connected in parallel with 20 series-connected solar cells [as in Fig. 1(b)].

In this article, the examined PV modules have three bypass diodes [as in Fig. 1(a)], and each diode is connected in parallel with 20 series-connected solar cells [as in Fig. 1(b)]. We experimented with three different PV modules to observe how severely bypass failure conditions can affect their performance. The second and third PV modules are working at normal conditions, and the first module is affected by one open-circuit bypass diode. The thermal image of the three tested PV modules, taken using FLIR TG165, is presented in Fig. 2. No hotspots are observed in PV#3 and PV#2, while PV#1 has an entire hotspot PV sub-string in the location where the bypass diode is in open condition. The temperature of the sub-string ranges from 55 °C to 60 °C, compared with adjacent non-hotspot PV modules of nearly 38 °C. This result confirms that defective bypass diodes can develop severe hotspots in the affected PV sub-string, and hence, degrade the output power of the PV module.

III. METHODOLOGY

A. Preliminary Analysis of PV Bypass Diodes

In this article, the behavior of three PV modules configured with different bypass diodes arrangements has been investigated, as illustrated in Fig. 3(a). PV#1 operates under normal operation, while PV#2 has one open bypass diode. The last module, PV#3, has one shorted bypass diode. The I - V and P - V curves were taken using a Solmetric PV analyzer instrument. The module's main electrical parameters at STC are, P_{MPP} : 220.1 W, V_{MPP} : 28.7 V, I_{MPP} : 7.67 A, V_{OC} : 36.7 V, and I_{SC} : 8.18 A.

All experiments apply the same amount of shade (40%) to modules with an opaque object (white sheet), since bypass diodes are activated if shading occurs. Tests were conducted with solar irradiance measured at 640 W/m² and module temperatures around 18 °C. The output measured I - V and P - V curves are presented in Fig. 3(b) and (c), respectively.

According to PV#1, The I - V or P - V curves show no losses in the I_{SC} or V_{OC} , while its P_{MPP} is equal to 121.6 W. However, we observe a significant drop of 4 A in the I_{SC} for the PV module with an open bypass diode (PV#2). This

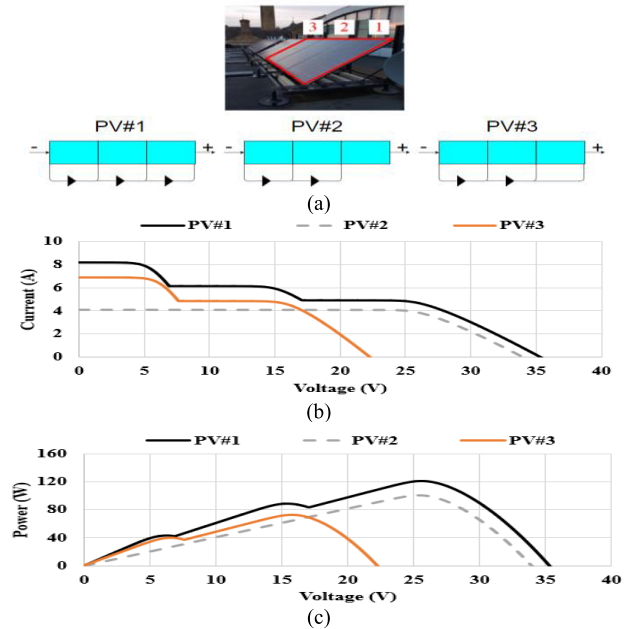


Fig. 3. (a) Examined PV modules with different bypass diode configurations (PV#1 normal, PV#2 with open bypass diode, PV#3 with short bypass diode). (b) Measured I - V curves. (c) Measured P - V curves.

result is expected because the PV sub-strings are connected in series. Therefore, due to the open bypass diode, the maximum generated current will be limited to the minimum value of all sub-strings. Subsequently, there is a 20.4 W loss in the output power ($P_{MPP} = 101.2$ W). In contrast, PV#3 experiences a drastic drop in its voltage because one of the sub-strings is now shorted due to the short-circuited bypass diode. In this case, the V_{OC} dropped by 13.7 V compared with PV#1, and the module $P_{MPP} = 72.4$ W.

B. Proposed ANN Model

A novel ANN model has been developed to detect faulty bypass diodes in PV modules. The ANN network architecture is presented in Fig. 4. The ANN is driven by three inputs, PV module output power, and; these inputs are then processed using one hidden layer, which consists of nine neurons. Extensive simulations were conducted in order to select the number of neurons. In MATLAB, 1–100 neurons were tested, and nine neurons were found to produce the best results.

As the number of PV modules in the system increased, the measured power and voltage rating shift is anticipated. It means that at STC where the solar irradiance is 1000 W/m², and the PV module temperature is 25 °C, a single PV module would generate 220 W, whereas two modules connected in series generate approximately double the power rating of 440 W. Therefore, in this work, a fixed bias in the ANN model to accommodate this requirement has been used. Note, the bias value is usually input using the graphical user interface (for example, 3× for three PV modules connected in series).

Each neuron in the hidden layer takes a formed linear combination of the outputs of the previous layer's neurons. This linear combination is weighted using the strength between the neurons (w_{ij}) and multiplied by both inputs (x_j).

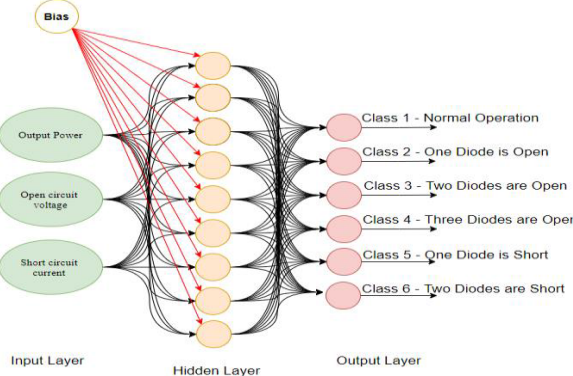


Fig. 4. Developed ANN model architecture.

An activation threshold (w_{j0}) was also assigned to each neuron. This process is expressed using (1) and (2) while utilizing the bias (b). Note: i is equal to the number of hidden neurons (1–9), j is equal to the number of inputs (1–3)

$$\sum_{j=1}^3 (w_{ij}x_j + w_{j0}) \quad (1)$$

$$b \times \sum_{j=1}^3 (w_{ij}x_j + w_{j0}). \quad (2)$$

The weighted activation process is then multiplied by the non-linear function f_1 as shown in (3), this is achieved using a sigmoid function, $f_1 = (1/(1 + e^{-x}))$. Finally, the output value of the hidden layers y_i is determined by (4)

$$f_1 \times \sum_{j=1}^3 (w_{ij}x_j + w_{j0}) \quad (3)$$

$$y_i = f(u) = \frac{1}{1 + e^{-\sum_{j=1}^3 (w_{ij}x_j + w_{j0})}}. \quad (4)$$

The output layer comprises six different classes, and each class corresponds to a specific condition. For example, if the predicted class of the ANN is “class 1,” the PV module is in normal operation mode, where no faulty bypass diode is detected. Subsequently, for “class 2,” one diode in the module is detected as open-circuit bypass diode mode. The description of each class is highlighted in Fig. 4.

The ANN characteristics are presented in Table I. The model comprises three inputs and six outputs using one hidden layer. The training process is supervised, meaning that we provided a set of input–output data of correct network performance. We randomly divided 70% of the samples for training, 15% for validation, and 15% for testing. Thus, we enable the validation of the desired topology. The training algorithm chosen is Levenberg–Marquardt, considering it is a faster algorithm for ANN networks of moderate sizes. The data were randomly selected for training, validating, and testing and all samples were normalized to 0–1. The dropout rate is used to prevent the ANN model from overfitting. The dropout rate for the input and hidden layers is 0.5. The process of dropout is driven by setting the weights to zero. In the training process, the number of iterations is 100, and the size of the batch is 10.

TABLE I

ANN MODEL CHARACTERISTICS

Parameter	Value
Input variables	3 (P_{MPP}, V_{OC}, I_{SC})
Output variables	6 (fault type)
Number of hidden layers	1
Number of neurons	8 + bias
Training process	Supervised (feedforward propagation)
Training algorithm	Levenberg–Marquardt
Activation function	Sigmoid
Type of division samples	Random
Training	70%
Validation	15%
Testing	15%
Normalization	(0,1)
Dropout rate for input layer	0.5
Dropout rate for hidden layer	0.5
Training iterations, Batch size	100, 10

It is unlike a situation where it is found that a PV module has faulty bypass diodes in open- and short-circuit conditions at the exact instant. Because when a bypass diode fails open, it can develop a hotspot in the sub-string, and subsequently, as time progresses, the diodes will be affected by excessive forward current and cause these to fail in open mode [6] as well. In contrast, when a bypass diode fails short-circuit, the voltage of the PV module will drop, so there will be little likelihood of diodes failing in the open mode at the same time.

PV#1 shown in Fig. 3(a) was left operating in the field for six days to record data samples for training and validating the ANN model. Each day a new faulty bypass condition was injected (i.e., day 1: normal operation, day 2: one diode is open, day 3: two diodes are open, etc.). From the measured/recorded samples, 80% were selected for training and 20% for validation. No data was spared for testing as the ANN model prediction accuracy will be examined using a different dataset, accurately representing the developed model’s precision.

The output confusion matrix of the ANN model is shown in Fig. 5(a). The accuracy of the ANN to predict the correct class is equal to 96.2% and 95.9%, respectively, while training and validating the model. In Fig. 5(a), the diagonal green boxes represent a correct fault classification, while any red boxes represent a false classification. In addition, the model took 61 iterations, (epoch) [see Fig. 5(b)], to achieve the minimum gradient of 0.31%. This means that the predicted classes of the confusion matrix are stopped after reprocessing the data 61 times. This test also indicated that no overtraining appears in the ANN since a minimal gradient was achieved (below 1%).

The summary of the proposed algorithm is presented in Fig. 5(c). The algorithm requires three inputs from the PV system, followed by processing the data into the ANN network, which was developed using MATLAB script. The ANN will then produce the output confusion matrix, followed by key indicators of the algorithm’s performance.

To evaluate the performance of the proposed algorithm, different terms have been used, and they are defined as follows:

- 1) *Bypass Diode Fault Detection Accuracy*: Closeness of the estimations to their true values; the model is more

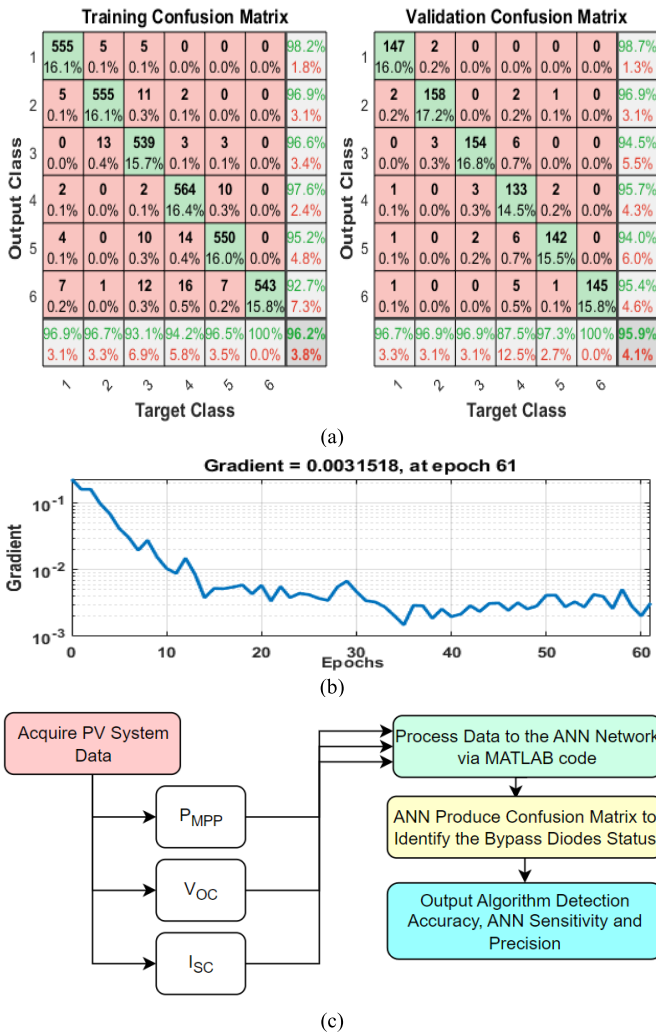


Fig. 5. (a) Output confusion matrix during the training and validation for the ANN model. (b) ANN network training state (epochs versus gradient). (c) Step-by-step summary of the proposed PV bypass diode detection algorithm.

accurate when it offers a smaller error, so approaching 100% accuracy rate implies that the algorithm can detect the PV bypass diodes faults with no error.

- 2) *Precision*: Closeness of repeated measurement results to each other. For example, when precision is above 90%, it implies that the collected samples from the experiment are very similar, and therefore, the ANN network can quickly identify the bypass diode's fault condition.
 - 3) *Sensitivity*: This is the metric that evaluates the ANN model's ability to predict the TPs of each available category. For example, a 90% sensitivity rate implies that the ANN model is sensitive enough to discover the PV bypass diode's fault categories (open circuit or short circuit).

IV. RESULTS

A. Experimental Setup Description

A practical step for these experiments comprising five series-connected PV modules to test the developed ANN model's accuracy (see Fig. 6). The modules are connected with

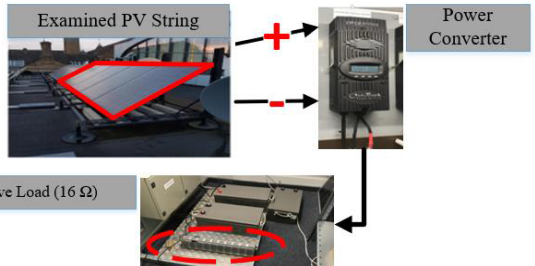


Fig. 6. Practical setup of the tested PV system.

TABLE II
ELECTRICAL PARAMETERS OF THE EXAMINED
PV SYSTEM AT STC CONDITIONS

Parameter	Value
Power at maximum power point (P_{MPP})	1100 W
Current at maximum power point (I_{MPP})	7.68 A
Voltage at maximum power point (V_{MPP})	143.25 V
Short circuit current (I_{SC})	8.10 A
Open circuit voltage (V_{OC})	183 V

a power converter to record the measured samples, including its main electrical parameters summarized in Table II. The PV system is connected with a purely resistive load ($16\ \Omega$). At STC conditions, the peak power of the system is 1100 W. Each PV module comprises three bypass diodes, and every single diode is connected in parallel with 20 series-connected solar cells.

B. Single PV Module in a PV System Affected by a Failure in the Bypass Diodes

The accuracy of the developed ANN model was obtained while running the PV system in different faulty bypass diode scenarios. On the first day, Fig. 7(a), the PV system operated under normal conditions until 8:59. Then, from 9:00 until 11:59, one bypass diode was open in one of the PV modules. Subsequently, an additional bypass diode was opened in the same PV module in the following four hours. In the last case, from 16:00 to 19:00, all bypass diodes were removed from the PV module.

It is worth noting that considerable fluctuations in solar irradiance affect the modules during the experiments; hence, the algorithm can detect the bypass diodes' faulty conditions. However, suppose there are no shading/overcasting/clouds available in the sky (known as clear sky condition). In that case, the algorithm cannot detect the faulty bypass diodes since all bypass diodes in this scenario will be anyways deactivated.

On the second day, in Fig. 7(b), a short-circuited bypass diode mode was investigated. A short-circuit occurred in the bypass diode of one PV module between 9:00 and 11:59. From 12:00 to 15:59, the same module had two short-circuited diodes. Consequently, the PV system operated normally between 5:00 and 8:59 and 16:00 and 19:00. As a result, 840 samples were collected per day on both days at a sampling rate of 1 sample/minute.

The output result of the ANN model, represented by the confusion matrix, is shown in Fig. 8. During day 1, Fig. 8(a),

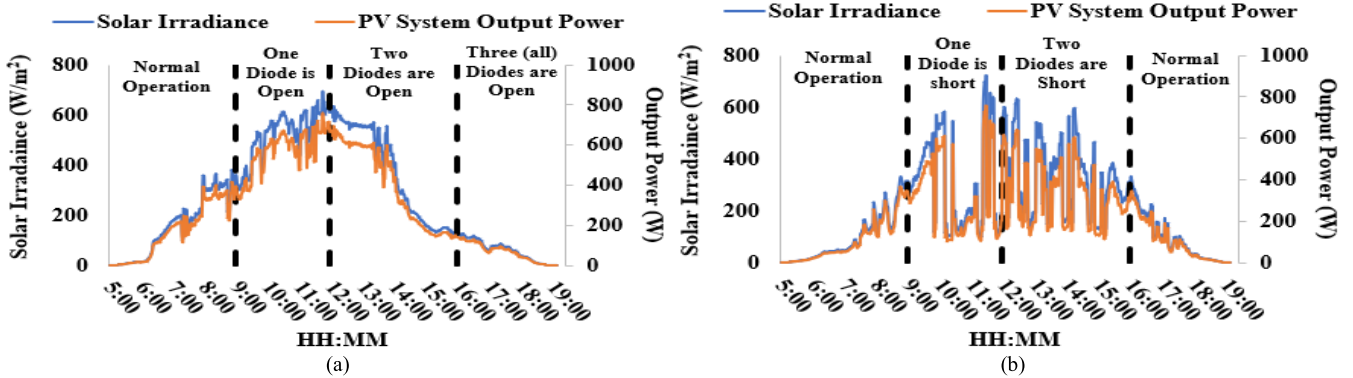


Fig. 7. Measured solar irradiance and PV system output power; for both days the PV average modules surface temperature was approximately 18 °C. (a) Day 1. (b) Day 2.

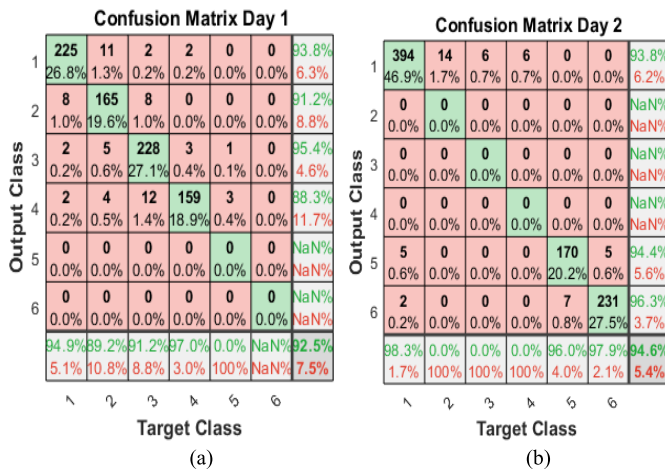


Fig. 8. Output ANN model confusion matrix. (a) Day 1. (b) Day 2.

the accuracy of detecting the actual fault condition is 92.5%. The following two compelling outcomes can be noticed in Fig. 8(a):

- 1) The number of samples classified as class 5 or 6 is limited (only 4) due to the fact that only short bypass diodes were examined in this experiment.
- 2) There is a standard misclassification between the classes. There were many samples misclassified into the nearest possible class. For example, observing the second row of the confusion matrix, 163 samples were correctly classified as class 2, while only eight were misclassified as class 1 or 3.

According to the ANN model prediction for the second day, Fig. 8(b), the overall bypass diode fault detection accuracy is 94.6%. Here, the following three significant features can be highlighted:

- 1) There were a limited number of samples (only 26) classified as classes 2, 3, and 4, as in this experiment only open bypass diodes were investigated.
- 2) Even though during this day there were rapid fluctuations in the solar irradiance [as seen previously in Fig. 7(b)], it did not affect the accuracy of predicting the correct class of the bypass fault condition.
- 3) Predicting the open bypass diode condition appears more accurate than the short condition because it is anticipated

TABLE III
PRECISION AND SENSITIVITY RATE OF EACH EXPERIMENTED CLASS

Class no.	TP	FP	FN	Precision (%)	Sensitivity (%)
1	225	12	15	94.9	93.7
2	165	20	16	89.2	91.1
3	228	22	11	91.2	95.4
4	159	5	21	96.9	88.3
5	170	7	10	96.0	94.4
6	231	5	9	97.8	96.3
Average				94.3	93.2

to see a more notable reduction in the output power of the PV system.

There are two additional metrics that can be calculated from the output confusion matrix, the first is the precision (ideal case = 100%) which indicates how many samples were identified as a fault and are correctly predicted. This metric is calculated using (5). The second metric is the sensitivity (ideal case = 100%) which is the ratio of TPs samples divided by the total number of TPs and false negatives. This metric is calculated using (6).

$$\text{Precision} = \frac{\text{TP}}{\text{TP} + \text{FP}} \quad (5)$$

$$\text{Sensitivity} = \frac{\text{TP}}{\text{TP} + \text{FN}} \quad (6)$$

where TP is the true-positive samples correctly classified, FP false-positive samples that are not faulty but have been classified as faulty, and FN is the false-negative samples that are faulty and have been identified as not faulty.

The summary of the precision and sensitivity of all classes is presented in Table III. The results show how well the developed ANN model predicts all the different classes. For example, the lowest precision and sensitivity are 89.2% and 88.3%, respectively, for classes 2 and 4.

C. Multiple PV Modules in a PV System Affected by a Failure in the Bypass Diodes (Static Fault)

In this section, the ANN model bias will be adjusted to the number of PV modules in the PV system, so the multiplication of the weighting by a factor of five is executed. In this case, the ANN confusion matrix will also be automatically synchronized to represent this change in the bias, hence,

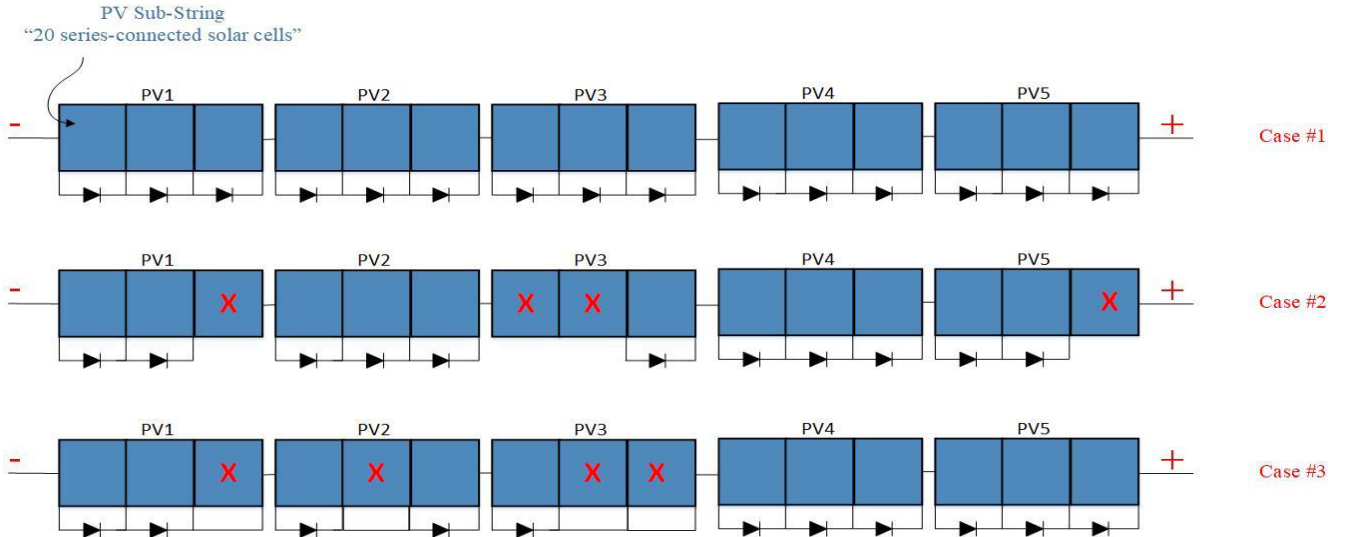


Fig. 9. Bypass diodes arrangement of the PV modules of the second experiment (static fault).

predicting the accurate number of bypass diodes failure in the PV system.

As shown in Fig. 9, three different case studies have been considered: case#1, the PV system is under a normal operation condition; in case#2 the PV system is affected by four open-circuit bypass diodes in different locations; and in the last case, case#3, the PV system is affected by four short-circuit bypass diodes. The output power against the solar irradiance in the three days of the experiment is shown in Fig. 10. During this experiment, the PV module's surface temperature was approximately 19 °C.

The ANN model requires the input of the other two parameters, V_{OC} and I_{SC} ; the log of these parameters is accessible via the power converter. In addition, the sampling rate remained at 1 sample/minute on the three days, resulting in 840 samples/day.

The output confusion matrix of the ANN model is shown in Fig. 10(d); here, nine classes are now present in the ANN as the bias multiplies the number of the class depending on the number of faulty bypass diodes in the PV system. Each class now represents the following conditions:

- 1) *Class 1:* Normal operation.
- 2) *Class 2:* One open-circuit bypass diode.
- 3) *Class 3:* Two open-circuit bypass diodes.
- 4) *Class 4:* Three open-circuit bypass diodes.
- 5) *Class 5:* Four open-circuit bypass diodes.
- 6) *Class 6:* One short-circuit bypass diode.
- 7) *Class 7:* Two short-circuit bypass diodes.
- 8) *Class 8:* Three short-circuit bypass diodes.
- 9) *Class 9:* Four short-circuit bypass diodes.

According to Fig. 10(d), the overall detection accuracy of the different cases is 93.1%. For case#1, 783 samples were correctly classified out of 840 (detection accuracy for class 1 = 93.2%). For case#2, the detection accuracy is 92.5%, where 777 samples are correctly classified. A detection accuracy of 93.5% is obtained for case#3. We observed that the increase in the number of faulty bypass diodes did not affect the genuine detection accuracy of the ANN model.

TABLE IV
PRECISION AND SENSITIVITY RATE OF EACH EXPERIMENTED CLASS

Class no.	TP	FP	FN	Precision (%)	Sensitivity (%)
1	783	49	57	94.1	93.2
5	777	0	63	100	92.6
9	785	0	55	100	93.4
Average				98.0	93.1

Furthermore, the location of the defective bypass diodes also does not affect the ANN model detection accuracy. We understand if the PV system consisted of 100 modules. Since the physical location and distribution of temperature, shading, and solar irradiance may differ, the ANN model's detection accuracy might decrease. Nevertheless, we demonstrated in this experiment that the developed approach can be applied to small-scale or residential PV systems.

Table IV summarizes the precision and sensitivity of the classes. Class 1 has the lowest precision at 94.1%, while the remaining classes have the highest precision at 100%. The average sensitivity of all classes is 93.1%.

The fault types (classes) were selected non-adjacently in this experiment to confirm how precisely (up to 100%) the ANN can predict the bypass diode fault. PV systems are often affected by faulty bypass diodes within the PV system that operates faulty for several days/weeks. While it is unlikely to see a PV system with multiple defective bypass diodes within a short period of time, it is an interesting topic worth investigating and will be discussed in Section IV-D.

The advantage of our developed model is that it can identify how many bypass diodes are defective in a PV system and provide the number and mode of the defective bypass diodes. The actual defective module, however, cannot be identified.

D. Multiple PV Modules in a PV System Affected by a Failure in the Bypass Diodes (Dynamic Fault)

In the previous experiment, the bypass diode failure did not change throughout the day, presenting a static fault. In this section, a dynamic fault identification will be performed in

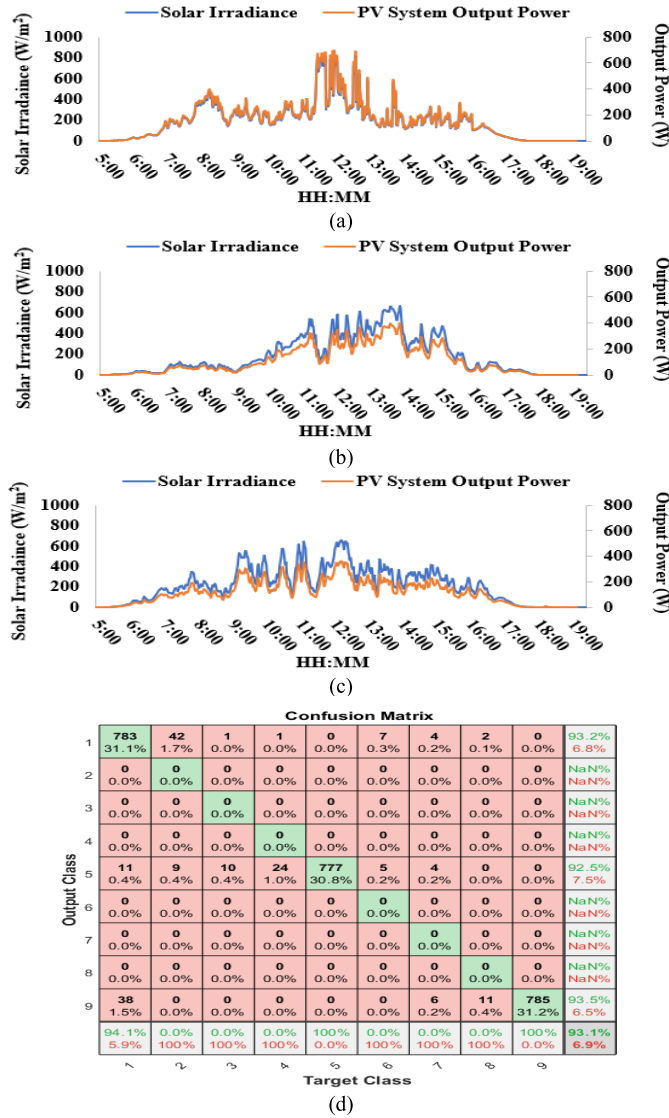


Fig. 10. Measured solar irradiance and PV system power, during the three days the average PV modules surface temperature was approximately 19 °C. (a) Day 1—case#1. (b) Day 2—case#2. (c) Day 3—case#3. (d) Output confusion matrix of the ANN model after processing the measured samples of the PV system obtained from the three case studies.

TABLE V
PRECISION AND SENSITIVITY RATE OF EACH EXPERIMENTED CLASS

Class no.	TP	FP	FN	Precision (%)	Sensitivity (%)
3	276	11	23	96.2	92.3
5	487	0	42	100	92.1
7	531	4	63	99.2	89.4
8	217	17	17	92.7	92.7
Average				97.0	91.6

the PV system as the conditions of the bypass diodes change throughout the day. Three different scenarios were considered, as shown in Fig. 11(a). PV system is affected by two open- and short-circuit bypass diodes between 5:00 and 9:59. From 10:00 to 13:59, the system was subjected to four open-circuit bypass diodes and three short-circuit bypass diodes. Last, the system was subjected to four and two open-circuit and short-circuit bypass diodes between 14:00 and 19:00.

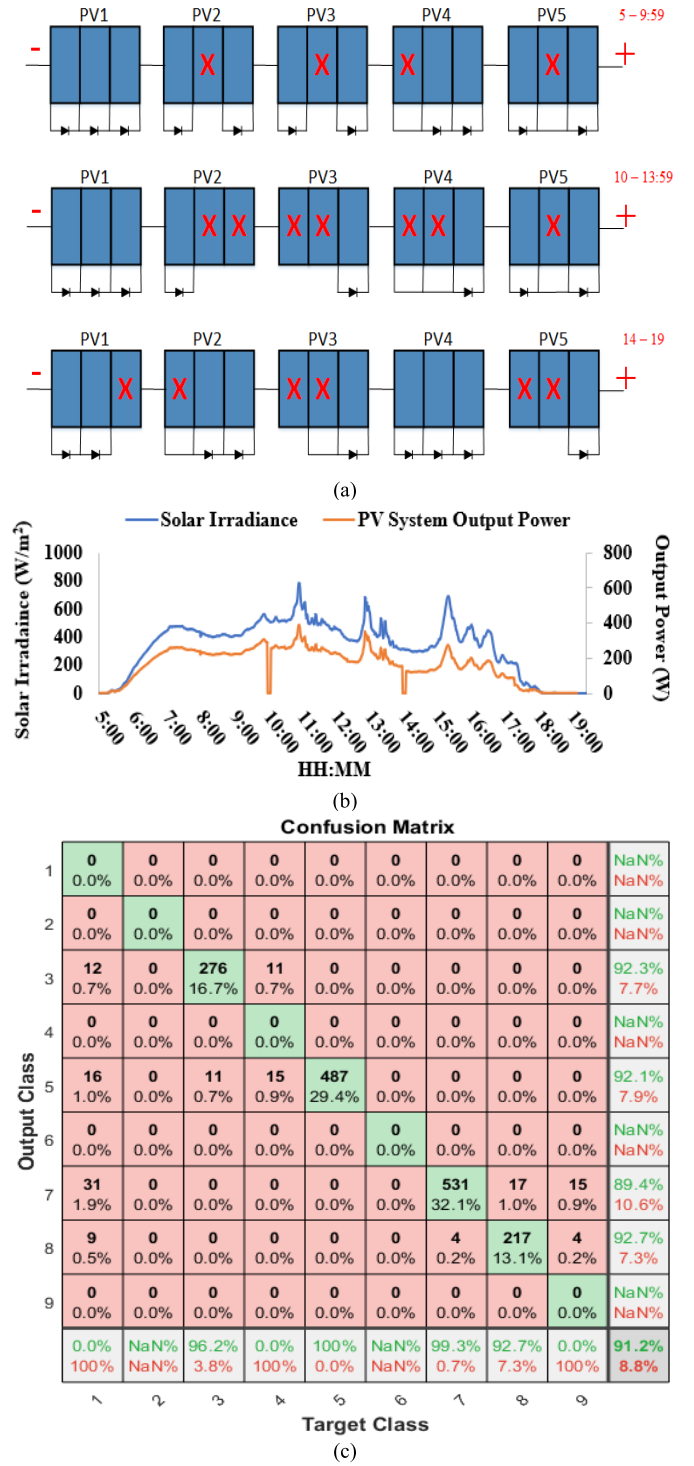


Fig. 11. (a) Bypass diodes arrangement of the PV modules of the third experiment (dynamic fault). (b) Measured solar irradiance and PV system power, the average PV modules surface temperature was approximately 22 °C. (c) Output confusion matrix of the ANN model after processing the measured samples of the PV system obtained from dynamic fault testing scenario.

The output measured solar irradiance and power of the PV system are shown in Fig. 11(b). The entire system was switched off during the test when changing the bypass diode failure condition, which can be seen in Fig. 11(b) where it shows zero PV output power at 10:00 and 14:00. The sampling rate for this test remained at 1 sample/minute, resulting in

TABLE VI
COMPARING OUR RESULTS WITH RECENT ALGORITHMS PRESENTED IN [17], [18], [19], [20], AND [21]

Reference	Year of Study	Bypass diode fault detection algorithm	Identify number of defective bypass diodes in a PV system	Bypass Diodes Fault Detection Accuracy (%)	
				Short	Open
[22]	2019	I-V curve identification	n/a	n/a	90
[23]	2020	Using thermal runaway testing, X-ray computed tomography (XCT), lock-in thermography	Yes	n/a	99
[24]	2021	I-V curve identification	Yes	n/a	90.2
[25]	2021	Remote anomaly detection of bypass diodes using deep neural network via UAV image detection using UAV drone	n/a	n/a	95
[26]	2021	Condition monitoring system based on radiometric sensors embedded in UAV drone	Yes	n/a	95
This work	2022	ANN model using three input parameters (P_{MPP}, V_{OC}, I_{SC})	Yes	93.6	93.3

299 samples for the first case and 234 and 295 samples for the second and third cases, respectively. We processed the data into the ANN in order to examine the fault prediction.

In terms of detection accuracy, we have achieved 91.2% (error or misclassification of the bypass diode's fault condition is only 8.8%). According to the results, class 8 had the best detection accuracy with 92.7%, while class 7 had the lowest with 89.4%.

Table V presents the precision and sensitivity of the classes calculated using (5) and (6). On average, the precision of the ANN model was 97.0%, while the sensitivity was 91.6%. Based on these results, it is apparent that the ANN model was correctly designed.

E. Comparative Study

A comparison is made between the findings of this study and those of recent studies (see Table VI) on the detection of PV bypass diodes' faults [22], [23], [24], [25], [26]. According to our knowledge, no previous work has been done on detecting short bypass diode fault identification (even though some articles claim that, but in reality, it is an open bypass diode). A majority of algorithms, such as [22] and [24], rely on detecting the PV system's I - V curve. Starting with this method is a great idea. It is, however, challenging to operate offline (using only the data from the power converters). In [23], the bypass diodes were detected using thermal testing; once again, the algorithm requires a physical inspection of the PV site, similar to those using drones for identifying failures in [25] and [26].

We present in this article an ANN algorithm that can efficiently operate with power converter data due to the fact that only three parameters are required (the output power, short-circuit current, and open-circuit voltage). Moreover, bias parameterization allows the model to be expanded by adding more bypass diodes classification if the PV modules in the system are increased. In both short- and open-circuit bypass diode detection, the average detection accuracy is over 93%.

V. CONCLUSION

This work reports an ANN-based model to detect short- and open-circuit bypass diode fault conditions in PV modules.

The advanced model only requires three inputs of the PV system: output power, short-circuit current, and open-circuit voltage, and it can identify the number of defective bypass diodes. Experimental validation on several PV modules has shown that the detection accuracy of the model is 93.6% and 93.3%, respectively, when detecting short- and open-circuit bypass diode conditions. It was also found by conducting various experiments that the average ANN network precision and sensitivity are equal to 96.4% and 92.6%, respectively. Our results are also compared with previously reported algorithms available in the literature; this work uniquely combines the short- and open-circuit bypass diode faulty conditions in an expandable model without using any drone-based or curve tracking of the PV system.

This work is significant in multiple ways: 1) the proposed model can detect open- and short-circuit bypass diodes simultaneously; 2) the model does not require any physical inspection of the PV system, such as thermal, electroluminescence or photoluminescence imaging, and finally; and 3) the proposed model is expandable, but here it is worth to note that if the model is used with a PV system comprising a large number of PV modules the accuracy is expected to drop slightly, so we highly recommend using the proposed solution with residential to medium-scale PV installations.

REFERENCES

- [1] *Snapshot of Global PV Markets*, IEA, Paris, France, 2021.
- [2] M.-C. Chang and S.-I. Liu, "An indoor photovoltaic energy harvester using time-based MPPT and on-chip photovoltaic cell," *IEEE Trans. Circuits Syst. II, Exp. Briefs*, vol. 67, no. 11, pp. 2432–2436, Nov. 2020, doi: [10.1109/TCSII.2020.2976760](https://doi.org/10.1109/TCSII.2020.2976760).
- [3] Y. Wang and B. Ren, "Fault ride-through enhancement for grid-tied PV systems with robust control," *IEEE Trans. Ind. Electron.*, vol. 65, no. 3, pp. 2302–2312, Mar. 2018, doi: [10.1109/TIE.2017.2740858](https://doi.org/10.1109/TIE.2017.2740858).
- [4] M. Dhimish and J. Kettle, "Impact of solar cell cracks caused during potential-induced degradation (PID) tests," *IEEE Trans. Electron Devices*, vol. 69, no. 2, pp. 604–612, Feb. 2022, doi: [10.1109/TED.2021.3135365](https://doi.org/10.1109/TED.2021.3135365).
- [5] S. Leva, M. Mussetta, and E. Ogliari, "PV module fault diagnosis based on microconverters and day-ahead forecast," *IEEE Trans. Ind. Electron.*, vol. 66, no. 5, pp. 3928–3937, May 2019.
- [6] A. Mehmood, H. A. Sher, A. F. Murtaza, and K. Al-Haddad, "A diode-based fault detection, classification, and localization method for photovoltaic array," *IEEE Trans. Instrum. Meas.*, vol. 70, pp. 1–12, 2021.

- [7] *Review on Failures of Photovoltaic Modules*, IEA, Brussels, Belgium, 2013.
- [8] B. P. Kumar, D. S. Pillai, N. Rajasekar, M. Chakkarapani, and G. S. Ilango, "Identification and localization of array faults with optimized placement of voltage sensors in a PV system," *IEEE Trans. Ind. Electron.*, vol. 68, no. 7, pp. 5921–5931, Jul. 2021, doi: [10.1109/TIE.2020.2998750](https://doi.org/10.1109/TIE.2020.2998750).
- [9] M. Jalil, H. Samet, T. Ghanbari, and M. Tajdinian, "An enhanced Cassie-Mayr-based approach for DC series arc modeling in PV systems," *IEEE Trans. Instrum. Meas.*, vol. 70, pp. 1–10, 2021, doi: [10.1109/TIM.2021.3124832](https://doi.org/10.1109/TIM.2021.3124832).
- [10] K. Li, S. Zhao, and Y. Wang, "A planar location method for DC arc faults using dual radiation detection points and DANN," *IEEE Trans. Instrum. Meas.*, vol. 69, no. 8, pp. 5478–5487, Aug. 2020, doi: [10.1109/TIM.2020.2966311](https://doi.org/10.1109/TIM.2020.2966311).
- [11] D. S. Pillai and N. Rajasekar, "An MPPT-based sensorless line-line and line-ground fault detection technique for PV systems," *IEEE Trans. Power Electron.*, vol. 34, no. 9, pp. 8646–8659, Sep. 2019, doi: [10.1109/TPEL.2018.2884292](https://doi.org/10.1109/TPEL.2018.2884292).
- [12] Z. Li, Y. Wang, D. Zhou, and C. Wu, "An intelligent method for fault diagnosis in photovoltaic array," in *Proc. Int. Conf. Electr. Inf. Technol. (ICEIT)*, 2017, pp. 10–16.
- [13] L. Bonisgrone, M. D. Rabhi, G. M. Tina, and A. E. Hajjaji, "Neuro-fuzzy fault detection method for photovoltaic systems," *Energy Proc.*, vol. 62, pp. 431–441, Jan. 2014.
- [14] M. S. Ramakrishna and S. N. Singh, "Modeling of PV system based on experimental data for fault detection using kNN method," *Sol. Energy*, vol. 173, pp. 139–151, Oct. 2018.
- [15] M. Hussain, M. Dhimish, S. Titarenko, and P. Mather, "Artificial neural network based photovoltaic fault detection algorithm integrating two bi-directional input parameters," *Renew. Energy*, vol. 155, pp. 1272–1292, Aug. 2020.
- [16] B. L. Aarseth, Å. F. Skomedal, M. B. Øgaard, and E. S. Marstein, "Detecting permanently activated bypass diodes in utility-scale PV plant monitoring data," *IEEE J. Photovolt.*, vol. 12, no. 5, pp. 1230–1236, Sep. 2022, doi: [10.1109/JPHOTOV.2022.3187381](https://doi.org/10.1109/JPHOTOV.2022.3187381).
- [17] M. Piliougue, R. A. Guejia-Burbano, and G. Spagnuolo, "Detecting partial shadowing and mismatching phenomena in photovoltaic arrays by machine learning techniques," *IEEE Open J. Ind. Electron. Soc.*, vol. 3, pp. 507–521, 2022, doi: [10.1109/OJIES.2022.3208140](https://doi.org/10.1109/OJIES.2022.3208140).
- [18] Y. Hayakawa, M. Baba, and N. Yamada, "Effect of bypass diode on power generation of three-dimensional curved Si photovoltaic module," *IEEE J. Photovolt.*, vol. 12, no. 1, pp. 388–396, Jan. 2022, doi: [10.1109/JPHOTOV.2021.3119254](https://doi.org/10.1109/JPHOTOV.2021.3119254).
- [19] A. Shabani and K. Mazlumi, "Evaluation of a communication-assisted overcurrent protection scheme for photovoltaic-based DC microgrid," *IEEE Trans. Smart Grid*, vol. 11, no. 1, pp. 429–439, Jan. 2020, doi: [10.1109/TSG.2019.2923769](https://doi.org/10.1109/TSG.2019.2923769).
- [20] G. Goudelis, P. I. Lazaridis, and M. Dhimish, "A review of models for photovoltaic crack and hotspot prediction," *Energies*, vol. 15, no. 12, p. 4303, Jun. 2022, doi: [10.3390/en15124303](https://doi.org/10.3390/en15124303).
- [21] C. Hernández et al., "Guidelines for protection against electric shock in PV generators," *IEEE Trans. Energy Convers.*, vol. 24, no. 1, pp. 274–282, Mar. 2009, doi: [10.1109/TEC.2008.2008865](https://doi.org/10.1109/TEC.2008.2008865).
- [22] M. Dhimish and Z. Chen, "Novel open-circuit photovoltaic bypass diode fault detection algorithm," *IEEE J. Photovolt.*, vol. 9, no. 6, pp. 1819–1827, Nov. 2019, doi: [10.1109/JPHOTOV.2019.2940892](https://doi.org/10.1109/JPHOTOV.2019.2940892).
- [23] C. Xiao, P. Hacke, S. Johnston, D. B. Sulas-Kern, C. Jiang, and M. Al-Jassim, "Failure analysis of field-failed bypass diodes," *Prog. Photovolt., Res. Appl.*, vol. 28, no. 9, pp. 909–918, Jun. 2020, doi: [10.1002/pip.3297](https://doi.org/10.1002/pip.3297).
- [24] S. Sarikh, M. Raoufi, A. Bennouna, and B. Ikken, "Characteristic curve diagnosis based on fuzzy classification for a reliable photovoltaic fault monitoring," *Sustain. Energy Technol. Assessments*, vol. 43, Feb. 2021, Art. no. 100958, doi: [10.1016/j.seta.2020.100958](https://doi.org/10.1016/j.seta.2020.100958).
- [25] M. Le, V. S. Luong, D. K. Nguyen, V.-D. Dao, N. H. Vu, and H. H. T. Vu, "Remote anomaly detection and classification of solar photovoltaic modules based on deep neural network," *Sustain. Energy Technol. Assessments*, vol. 48, Dec. 2021, Art. no. 101545, doi: [10.1016/j.seta.2021.101545](https://doi.org/10.1016/j.seta.2021.101545).
- [26] I. S. Ramírez, B. Das, and F. P. G. Márquez, "Fault detection and diagnosis in photovoltaic panels by radiometric sensors embedded in unmanned aerial vehicles," *Prog. Photovolt., Res. Appl.*, vol. 30, no. 3, pp. 240–256, Mar. 2022, doi: [10.1002/pip.3479](https://doi.org/10.1002/pip.3479).



Mahmoud Dhimish (Member, IEEE) received the M.Sc. degree in communications and electronics engineering and the Ph.D. degree in renewable energy engineering from the University of Huddersfield, Huddersfield, U.K., in 2016 and 2018, respectively.

In May 2018, he joined the University of Huddersfield, as a Lecturer and then Senior Lecturer of electronics and control systems engineering. Since September 2021, he has been working as an Assistant Professor of electrical engineering and the Head of Photovoltaics Laboratory, University of York, York, U.K. He has published over 70 articles in these areas. He was ranked among the top five U.K. scientific academics by a leading index in October 2022. His main research interests include photovoltaic (PV) systems operation (faults, cracks, hotspots, etc.), AI/ML adaptation, power electronics, and fault-tolerant algorithms.



Andy M. Tyrrell (Life Senior Member, IEEE) received the degree (Hons.) in electrical and electronic engineering and the Ph.D. degree in electrical and electronic engineering from Aston University, Birmingham, U.K., in 1982 and 1985, respectively.

In April 1990, he joined the Department of Electronic Engineering, University of York, York, U.K. He is also the Head of the Department of Electronic Engineering, University of York. This work has included the creation of an embryonic processing array, intrinsic evolvable hardware systems, and autonomous robot evolutionary systems. He has published over 350 articles in these areas. His main research interests include the design of biologically inspired architectures, evolutionary robotics, evolvable hardware, and novel engineering design methods.

Dr. Tyrrell is a Fellow of IET. He was promoted to the Chair of Digital Electronics at the Department of Electronic Engineering, University of York, in 1998.